PAPER

Evaluating perovskite solar panels for thermal stability and inclination performance through finite element modelling

To cite this article: Ranfu Wang *et al* 2024 *Eng. Res. Express* **6** 025327

Engineering Research Express

PAPER

Evaluating perovskite solar panels for thermal stability and inclination performance through finite element modelling

Ranfu Wang[1,2], **Xinzhi Liu**[1,3] and **Suhaidi Shafie**[3]

[1] Department of Physics, Hong Kong Baptist University, Kowloon Tong, Kowloon, Hong Kong SAR 999077, People's Republic of China
[2] China Three Gorges Renewables Group Co Ltd, Zhejiang Branch, 310000, Hangzhou, People's Republic of China
[3] Department of Electrical and Electronic Engineering, Universiti Putra Malaysia, 43400 Selangor, Malaysia

E-mail: berryxinzhiliu@hotmail.com

RECEIVED
24 February 2024

REVISED
17 April 2024

ACCEPTED FOR PUBLICATION
25 April 2024

PUBLISHED
7 May 2024

Keywords: solar panel, finite element modelling, perovskite solar panel

Supplementary material for this article is available online

Abstract

This paper presents a foresight simulation of perovskite solar modules, focusing on their behavior under different wind velocities and the thermal effects of varying solar irradiance conditions. Despite the burgeoning interest in Perovskite solar panels (PSPs) due to their lower material costs and promising efficiencies, there exist significant research gaps, particularly in the interaction between wind flow and thermal variations, as well as the performance dynamics under distinct wind velocities. To address these gaps, Finite Element Modelling (FEM) simulations were conducted to analyze the thermal stability and wind stress resistance of PSPs, employing a structural design analogous to commercial silicon PV panels. The simulations revealed that the implementation of a cooling system effectively lowered the average temperature of the perovskite layer by a factor of 2.46, significantly reducing the risk of thermal degradation. Additionally, wind stress simulations demonstrated a direct proportionality between the vertical pressure on the panels and their inclination angles, suggesting that lower angles could minimize wind-induced damage while considering daily solar azimuth. The study's outcomes contribute to the understanding of PSPs' mechanical and thermal resilience, proposing an optimized design approach for enhanced durability and efficiency in real-world applications. However, the segregation of thermal and wind flow simulations suggests an area for further integrated studies to fully comprehend the simultaneous effects of environmental factors on PSP performance.

1. Introduction

Solar photovoltaic (PV) technology has emerged as a cornerstone of renewable energy, offering a sustainable and abundant source. Its widespread adoption is not limited by geography, making it a crucial component of urban electricity networks worldwide. The International Energy Agency (IEA) highlights the rapid growth in solar power capacity, with utility-scale solar power increasing from 63.0 GW to 150.8 GW and distributed solar power from 35.0 GW to 136.2 GW, as shown in figure 1. This expansion signifies solar PV's critical role in the ongoing transformation of the global energy landscape [1]. Notably, the flexibility of solar PV systems enables their integration into diverse settings, from urban rooftops to vast ground-mounted installations, showcasing their broad applicability and potential in addressing diverse energy demands. Despite the prevalence of crystalline silicon-based solar cells, their power conversion efficiency (PCE) is nearing the theoretical maximum as delineated by the Shockley–Queisser limit [2]. The high fabrication costs, the expense of raw materials, and their capped efficiency highlight the need for innovative materials in solar cell technology.

Illustrated in figure 2(a), PSPs stand out among experimental solar cell technologies due to their unique crystal structure, akin to the mineral $CaTiO_3$ [3]. PSPs have attracted considerable interest for their exceptional efficiency and economical production techniques. Central to their functionality are the perovskite materials, comprising a versatile array of compounds, each with distinct properties [4]. Prominent among these are

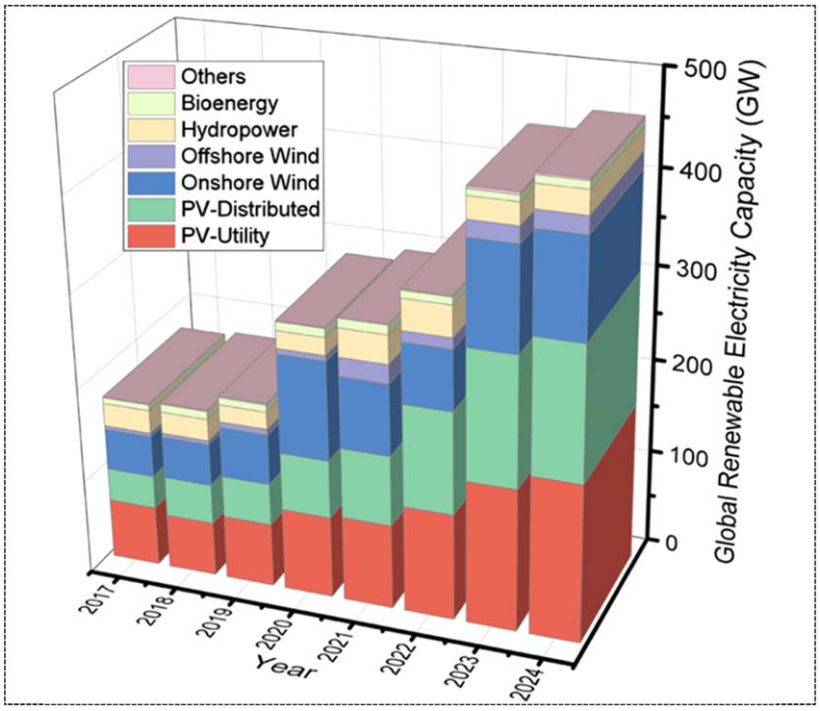

Figure 1. Evolution of global renewable energy capacity.

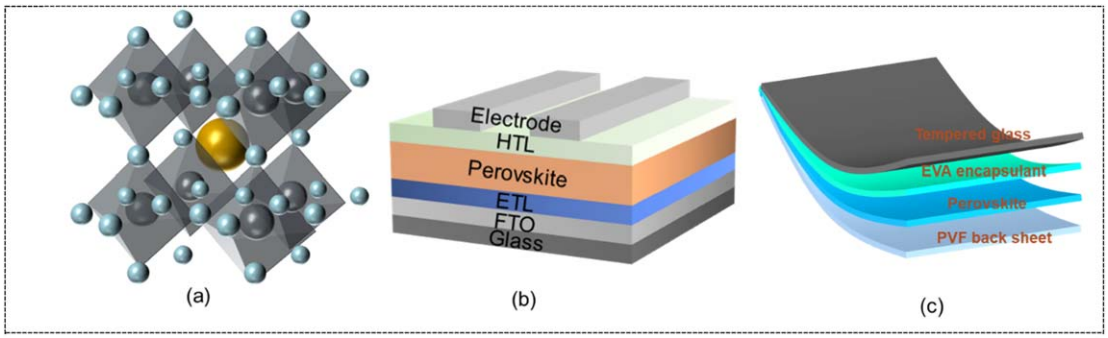

Figure 2. (a) 3D crystalline structure of a typical Perovskite crystal, (b) experimental perovskite cell structure, (c) proposed commercial perovskite solar panel layers.

lead-based perovskites such as methylammonium lead iodide ($MAPbI_3$), formamidinium lead iodide ($FAPbI_3$), cesium lead iodide ($CsPbI_3$), and methylammonium lead chloride ($MAPbCl_3$). $MAPbI_3$ is especially celebrated for its optimal bandgap and superior absorption efficiency, which makes it a staple in high-efficiency Perovskite Solar Cells (PSCs) [5]. $FAPbI_3$ is valued for its thermal stability and appropriate bandgap, enhancing its suitability for photovoltaic applications. Conversely, $CsPbI_3$ is distinguished by its stability at room temperature in its black phase, and $MAPbCl_3$ is being investigated for its potential in tandem cell configurations due to its broader bandgap [6].

When compared to traditional solar cells such as monocrystalline silicon, polycrystalline silicon, and gallium arsenide (GaAs), PSPs offer numerous advantages. These include lower material and fabrication costs, optimal film thickness around 500 nm, potential for scalable manufacturing processes, and the flexibility of solar modules, as depicted in figure 2(b) [7, 8].

Traditionally, PSPs are quite thin and delicate, necessitating their encapsulation within a protective structure. This typically involves a transparent front sheet, often made of glass, and a back sheet, which can either be glass or a durable plastic material. Furthermore, it is essential for the perovskite cells to be shielded by EVA (ethylene-vinyl acetate) PB (polybutylene)-absorbing encapsulants and reinforced with a metal frame for additional durability. In the context of constructing detailed laminated structures for accurate heat flux simulations, the design of perovskite solar cells incorporates several layers. These include an aluminum frame

for structural support, tempered glass for protection, lead-absorbing EVA encapsulants on both sides to safeguard against potential lead leakage, a perovskite layer at the core for energy conversion, and a PVF (polyvinyl fluoride) back sheet at the base to complete the assembly, as shown in figure 2(c). This layered configuration is akin to the commercial silicon PV panels, critical for longevity and robustness [9, 10].

In the context of commercializing perovskite-based solar panels, the implications of manufacturing discrepancies and fabrication tolerances are crucial in defining their ultimate performance and dependability. At the experimental laboratory level, the susceptibility of PSPs to variations in layer thickness, compositional accuracy, and environmental conditions during production markedly impacts their operational efficiency and stability [11–13]. Deviations such as uneven layer deposition or minor changes in the stoichiometry of the perovskite compounds can introduce defects that serve as recombination centers, detrimentally affecting the power conversion efficiency [8, 14]. Furthermore, the scalability of manufacturing processes poses a challenge, as the transition from laboratory-scale to industrial-scale production often amplifies these variances [15].

Numerous studies have employed Finite Element Modelling (FEM) and various simulation techniques to explore the dynamics of solar photovoltaic panels. Hasan *et al* (2012) developed a Finite-Element model for a 36-cell PV module using 2D layered shell elements in ANSYS. Their simulations, conducted over a 24-hour constant temperature scenario, aimed to assess the integrity of cell lamination under standardized industrial temperature cycles. The significant finding of this study was the identification of critical mechanical interactions between cells, although it did not address the impacts of variable solar irradiance and wind-induced stresses, assuming uniform temperature conditions throughout [16]. Lee and Tay (2012) executed a Finite Element thermal analysis on an operational PV module to examine the temperature distribution across its layers and surfaces. They discovered that the operational temperatures of photovoltaic modules are profoundly influenced by the materials of the frame and the dimensions of the panels. This analysis provides essential insights into thermal management within PV modules, though it neglected the effects of panel inclination angles and wind flow, assuming a static horizontal placement [17]. Leow *et al* (2016) analyzed the effect of wind speed on the temperature distribution of solar panels. Their study highlighted how increased wind speeds could moderate panel temperatures effectively, yet failed to consider the variations in panel inclination angles which could significantly alter these effects [18].

Recent research has further explored the application of FEM in studying solar panels. Laha *et al* (2022) concentrated their simulation efforts on the critical aspect of operating temperature, which has a significant impact on both the efficiency and longevity of solar panels [19]. They observed that severe self-heating could drastically diminish panel efficiency and shorten its lifespan. In their study, numerical experiments were conducted by varying mesh thickness from 0.5 m to 0.05 m. The results showed that at a mesh size of 0.5 m, the maximum temperature reached was 66.974 °C, corresponding to a solar efficiency of 12.168%. However, with the integration of a cooling system, the efficiency improved to 13.05%, while the temperature decreased to 53.98 °C. This study highlights the importance of effective temperature management in optimizing solar panel performance. Nonetheless, it simplified the model by focusing solely on thermal temperature distribution, without considering multiple variables such as external wind flow. Nivelle *et al* (2021) conducted a review of FEM simulations focusing on the stress and strain impacts on photovoltaic modules, detailing the thermo-magnetic behaviors [20]. While this work primarily examined commercial solar panel structures by elucidating their mechanical behavior, it devoted less attention to emerging solar cell materials and the integration of multiple flow conditions within a single simulation setup.

Despite numerous contributions through FEM simulations in understanding solar panel temperature and wind flow, two major research gaps remain prevalent. First, the majority of existing studies focus exclusively on conventional silicon modules, largely overlooking emerging technologies such as perovskite solar cells and III-IV compound semiconductors, like GaAs. Second, these studies tend to isolate variables, whereas real-world scenarios typically involve multiple interdependent environmental factors [9].

This paper seeks to bridge these gaps by examining the behavior of perovskite solar modules under varying wind velocities and their thermal stability under specific solar irradiance conditions. Given the nascent stage of perovskite panel commercialization, we reference the established mechanical structures of silicon panels, employing EVA Pb-absorbing encapsulants and a metal frame for support. The design incorporates an aluminum frame, tempered glass, lead-absorbing EVA encapsulants on both sides, a perovskite layer, and a PVF back-sheet at the base, with dimensions set at 1.065 m $\times$ 0.900 m $\times$ 0.054 m. The paper is structured as follows: section 2 presents the fundamental concepts related to simulation parameters, including isotropic thermal conductivity, pertinent parameters, and principles of solar atmospheric conditions. Section 3 describes the detailed simulation design, section 4 presents the results and discussions, and the conclusion synthesizes the findings, offering a comprehensive summary of the study.

Table 1. Parameters for simulating thermal stability performance of perovskite solar panels.

Material Field Variables	Isotropic thermal conductivity K(W/m*K)	Density ρ(kg/m^2)	Specific Heat Cp (J/kg*K)
Tempered Glass	1.8	3000	500
EVA Encapsulant	0.35	960	2090
Perovskite cell	0.59	4000	308
PVF back sheet	0.2	1200	1250

2. Fundamentals and selection of simulation parameters

In this section, the focus is on modelling a perovskite photovoltaic solar panel using FEM simulation. Materials are identified as isotropic when their properties remain constant regardless of directionality. A comprehensive understanding of the properties of each layer within the photovoltaic collector is essential prior to the assembly of the layers. Among these properties, thermal conductivity is paramount; it quantifies a material's capacity for heat transfer and is indispensable for performing transient heat transfer analyses. Additionally, the mass density per unit volume for each layer is crucial for considerations pertaining to thermal elements. Moreover, the specific heat capacity—defined as the amount of energy required to elevate the temperature of a unit mass of the material by one degree Celsius—is critical for elements considered as fluids in thermal analyses that incorporate the effects of fluid dynamics.

In this study, parameters for FEM simulation are illustrated in table 1 including mass density, isotropic thermal conductivity, and specific heat for materials such as EVA encapsulant, PVF back sheet, and tempered glass are referenced [17]. The thermal conductivity of perovskite, which varies with temperature from 160 K to 400 K, encompasses both the tetragonal phase (160–330 K) and the pseudo-cubic phase (>330 K). Notably, a low thermal conductivity of 0.59 W m^{-1}*K^{-1} characterizes the tetragonal phase at room temperature, contrasting with a higher value of 1.80 W m^{-1}*K^{-1} observed in the pseudo-cubic phase at 330 K [21]. This disparity is attributed to the tetragonal perovskite's low group velocity of acoustic phonons and significant anharmonicity, which contribute to its relatively low thermal conductivity. The perovskite is thus considered to demonstrate favorable phase stability, evidenced by a thermal stability of 0.59 W m^{-1}*K^{-1}. Within perovskite solar cell configurations, metal oxides such as TiO_2 are employed as electron transporting layers alongside the perovskite crystal and metal electrode. The estimated density for the equivalent solar panel is established at 4000 kg m^{-3}. Furthermore, research has determined the specific heat capacity of $MAPbI_3$ perovskite to be 308 J*kg^{-1}K^{-1}, a value considerably lower than that of silicon crystals. The Steady-State Thermal analysis is subsequently chosen to assess the thermal flux stability following the completion of material settings.

Before defining the boundary conditions for the simulation, it is essential to determine the heat flux on the outer surface of the PV panel, with estimations made for clear-sky radiation conditions. The declination angle (δ) can be calculated using the approximate equation provided by copper [22]:

$$\delta = 23.45 \ \sin\left(360 \times \frac{284 + n}{365}\right) \tag{1}$$

In this context, the declination angle is selected to be +14.88°. For a horizontal collector, the angle of incidence corresponds to the sun's zenith angle, denoted as θ_Z [23, 24]:

$$\cos\theta_z = \cos\phi \ \cos\delta \ \cos\omega + \sin\phi \ \sin\delta \tag{2}$$

In this formula, ω signifies the hour angle, reflecting the sun's angular displacement east or west of the local meridian, a result of Earth's rotation on its axis at a rate of 15° per hour. In the morning, this value is negative, transitioning to positive in the afternoon. Latitude (Φ) represents the angular position north or south of the Equator, with northern latitudes assigned positive values. When the hour angle, ω, is −7.5, the cosine of the zenith angle calculates to 0.7625. Based on the literature review, the atmospheric transmittance for beam radiation equation could be expressed as [22]:

$$\tau_b = a_0 + a_1{*}\exp\left(\frac{-k}{\cos\theta_z}\right) \tag{3}$$

The constants a_0, a_1, and k, which pertain to a standard atmosphere with 23 km visibility, are derived from $a_0{}^*$, $a_1{}^*$, and k^*. These values are provided for altitudes below 2.5 km, assumed to be in flatlands in Hong Kong:

$$a_0{}^* = 0.4237 - 0.00821(6 - A)^2 = 0.1316 \tag{4}$$

$$a_1{}^* = 0.5055 + 0.00595(6.5 - A)^2 = 0.7542 \tag{5}$$

Table 2. Correction factors for climate types.

Climate Type	r_0	r_1	r_k
Tropical	0.95	0.98	1.02
Midlatitude Summer	0.97	0.99	1.02
Subarctic Summer	0.99	0.99	1.01
Midlatitude Winter	1.03	1.01	1.00

$$k^* = 0.2711 + 0.01858(2.5 - A)^2 = 0.348 \tag{6}$$

Correction factors are applied globally in table 2, as outlined in the reference [25]:
The latitude of Hong Kong is close to tropical. Therefore:

$$a_0 = r_0 \times a_0{}^* = 0.125 \tag{7}$$

$$a_1 = r_1 \times a_1{}^* = 0.739 \tag{8}$$

$$k = r_k \times k^* = 0.39168 \tag{9}$$

$$\tau_b = a_0 + a_1 \ * \ \exp\left(\frac{-k}{\cos\theta_z}\right) = 0.125 + 0.739 \times e^{\left(\frac{-0.39168}{0.7625}\right)} = 0.5671 \tag{10}$$

Additionally, Gon represents the extraterrestrial radiation incident on a plane normal to the radiation on the nth day of the year:

$$G_{on} = G_{sc}\left(1 + 0.033 \ \cos\frac{360n}{365}\right) = 1397 \quad w/m^2 \tag{11}$$

The solar radiation is then:

$$E = 1397\frac{w}{m^2} \times 0.5671 = 792.234\frac{w}{m^2} \tag{12}$$

The component on a horizontal plane is as follows:

$$E_{horizontal} = 792.234\frac{w}{m^2} \times 0.7625 = 604\frac{w}{m^2} \tag{13}$$

Upon determining the solar irradiance parameter and setting the heat flux at 604 W m^{-2}, convection is applied to the top surface of the solar panel. This is followed by incorporating temperature-dependent properties of stagnant air into the layers, thereby generating the heat flux.

3. FEM simulation design

As depicted in figures 3(a) and (b), the mechanical layout of PSP module was designed in ANSYS Fluent, featuring eight cells per panel. The dimensions of the solar cell model are 1.065 m × 0.900 m × 0.054 m. Each layer's geometry is individually laminated [26].

3.1. Design of PSP thermal stability performance simulation

As the previous chapter discussed, based on the geographical coordinates of Hong Kong, the solar radiation at noon on July 1st is calculated to be 604 W/m^2 on a horizontal surface. Additionally, the convection coefficients for both the frame and the glass are estimated at 7.6 W/m^2·°C. Consequently, a heat flux of 604 W/m^2 and a convection value of 7.6 W/m^2·°C are applied to the solar panel model. Moreover, an initial temperature of 27 °C (300 K) is uniformly established across the model.

3.2. Design of wind loads at different inclination angles

In addition to temperature fluctuations, solar panels are subject to the effects of natural wind. The force exerted by strong winds can lead to serious mechanical issues in solar panels, making the understanding of wind flow and its interaction with the panels crucial. For this reason, the FEM simulation is employed to model the wind load on PSPs at varying inclination angles under steady-state conditions.

Based on the wind pressure distribution report for Hong Kong, the average basic wind pressure over the past decade has been estimated at approximately 0.5 kN/m^2, with an annual average wind speed of about 30.53 m s^{-1}. Given the potential for excessive wind force to damage solar panels, it is crucial to conduct simulations and analyses of the wind load on solar panels. To this end, FEM simulation is employed to model the impact of wind load on a solar panel at various angles of inclination. A cubic computational air domain, with dimensions of 2.5 m × 2.5 m × 2.5 m, is created for the geometry module, positioning the solar panel centrally

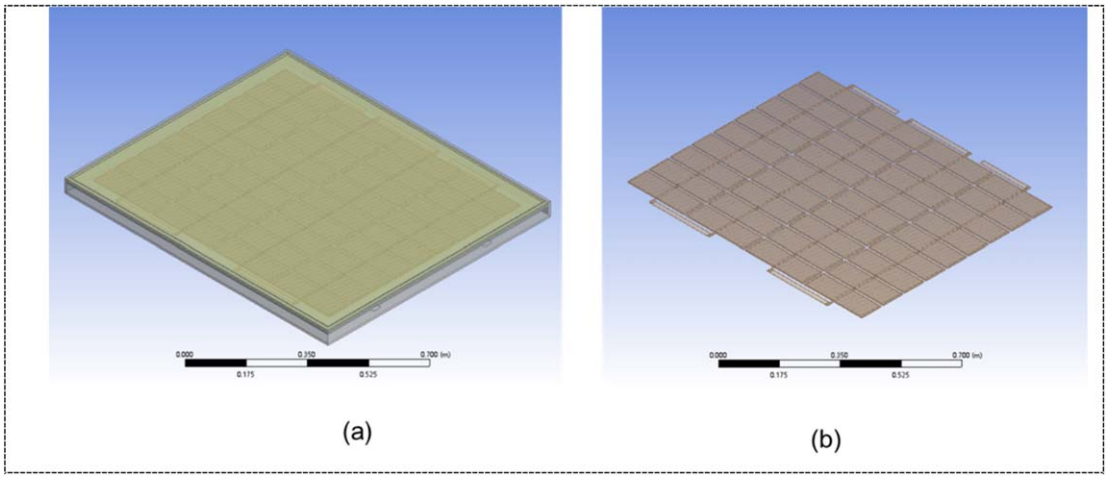

Figure 3. Geometry of (a) the PSP mechanical layout and (b) PSP layer with individual cells.

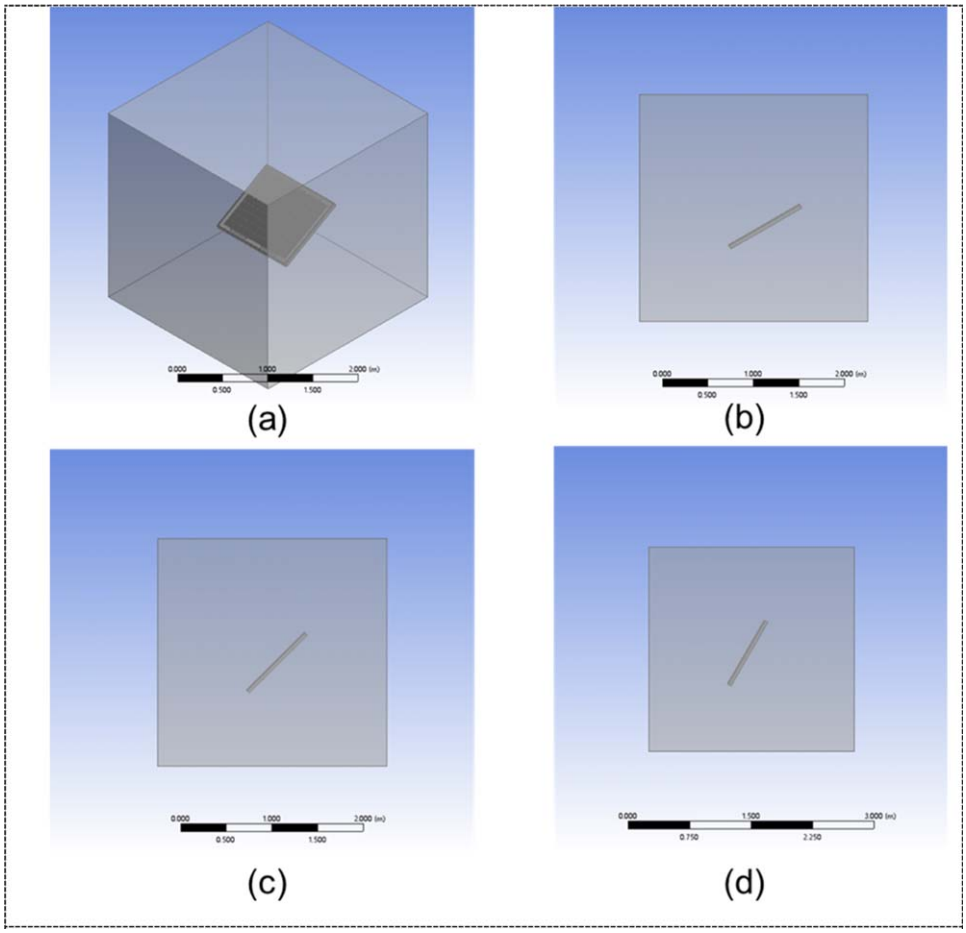

Figure 4. Geometry of (a) the Computational Domain with Dimensions; (b) Solar Panel Inclined at 30° within the Domain; (c) Solar Panel Inclined at 45° within the Domain; (d) Solar Panel Inclined at 60° within the Domain.

to enhance the simulation's efficiency. Concurrently, the solar panel's inclination angle is adjusted to 30°, 45°, and 60° relative to the horizontal plane for comparative analysis. Illustrations are provided in figure 4: figure 4(a) depicts the computational domain with dimensions, while figures 4(b) to (d) demonstrate the solar panel at various inclination angles, respectively.

Mesh generation is a critical step in finite element simulations, particularly for PSPs and their surrounding domains. The mesh is meticulously designed to accurately represent curvature and proximity features. To

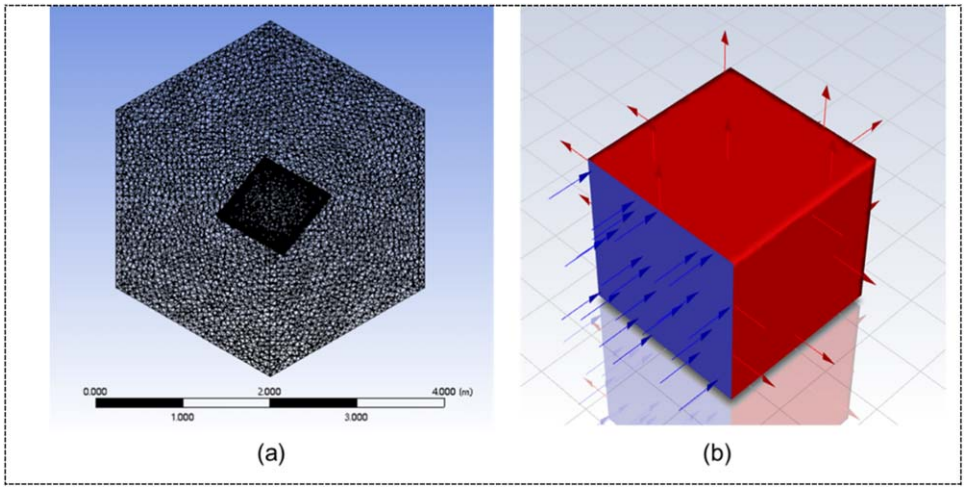

Figure 5. Geometry of (a) mesh elements setting; (b) inlet, floor and outlet setting of the mesh with air flow directions.

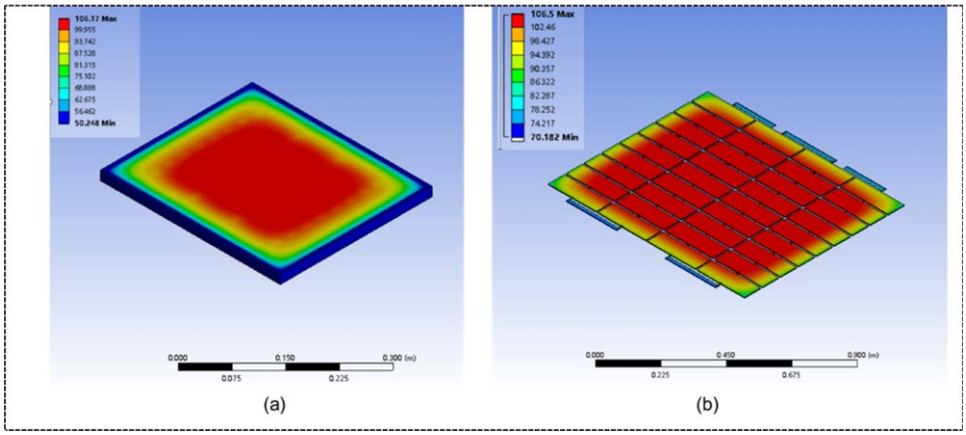

Figure 6. Temperature distribution across (a) the glass layer and (b) the perovskite PV layer without an air-cooling system.

enhance the resolution of the solar panel's boundary layer, inflation layers are strategically added. The resulting mesh model comprises 196,047 elements and 42,535 nodes, with the maximum skewness maintained below 0.80 as shown in figure 5(a). The naming convention for the model's faces includes designating the front face as 'Inlet,' the bottom face as 'Floor,' and all other faces as 'Outlet.' The chosen Viscous Model is the standard k-epsilon model, known for its reasonable accuracy in simulating the mean flow characteristics of turbulent flow conditions. Consequently, the material for the fluid domain is specified as air as shown in figure 5(b), reflecting the focus on wind loading effects on the solar panel. The velocity magnitude at the inlet is set to 5.81 m s^{-1}, aligning with the average wind speed in Hong Kong, serving as a practical approximation. Furthermore, the gauge pressure across all boundaries is maintained at zero, ensuring that the absolute pressure matches the operating pressure and situates the simulation under the standard atmospheric pressure of 101,325 Pa. The setup of the model is then initialized, and the solution process begins, with the number of iterations fixed at 100.

4. Results and discussion

4.1. Temperature variation of PSP module thermal distribution under fixed irradiance

The simulation results in figures 6 and 7 reveal that within the solar panel model, the top glass layer exhibits the highest temperature, whereas the lowest temperature is found in the aluminum frame. This discrepancy is attributed to aluminum's superior thermal conductivity relative to other materials in the model. Furthermore, the combined effects of conductive and convective heat transfer efficiently dissipate the heat generated by the solar panel model into the surrounding environment at an accelerated rate. For the perovskite cell layer, temperatures range from a maximum of 106.5 °C to a minimum of 70.6 °C, as shown in figure 8. These

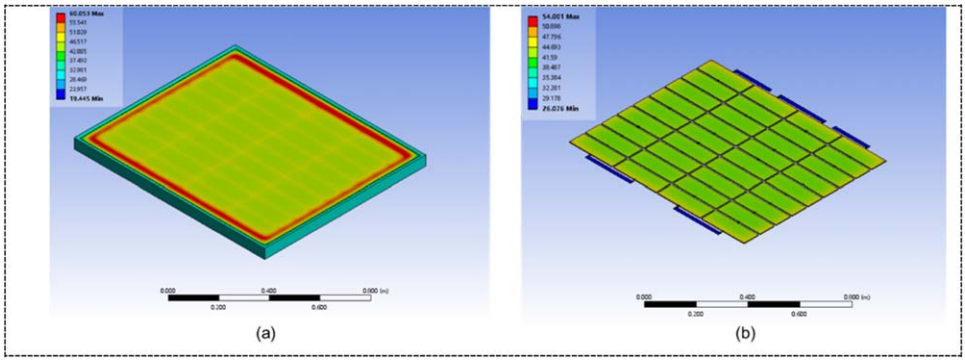

Figure 7. Temperature distribution throughout (a) the glass layer and (b) the perovskite layer within air cooling.

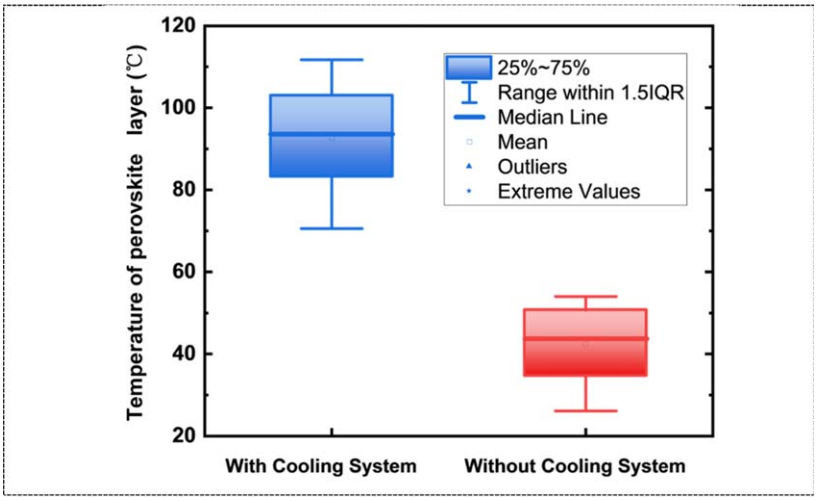

Figure 8. Scattered boxplots of perovskite layer temperature within and without cooling system.

temperatures remain below the perovskite's thermal tolerance threshold. Nonetheless, the uneven distribution of heat dissipation, due to thermodynamic properties, could potentially lower PSP conversion efficiency if such high temperatures are sustained over extended periods.

To maintain power output by cooling PSPs, air serves as the chosen cooling medium, directed from the left side of the PV panel and exiting through an air duct on the right. The wind at the inlet is consistently supplied at a velocity of 1 m/s. The temperature of the solar panel is notably affected by the velocity of the wind, as illustrated in figure 7. This phenomenon occurs because the flow of wind velocity facilitates a cooling effect on the surface of the solar panel model, enabling the dissipation of heat generated by the panel into the surrounding environment. Thus, the air-cooling system proves to be effective in lowering the operating temperature of the solar panel, ensuring it functions efficiently at reduced temperatures. Referring to figure 8, it is noted that the maximum temperature of the perovskite layer decreased to 54.0 °C, while the minimum temperature reached 41.5 °C. The implementation of the cooling system effectively reduced the average temperature of the perovskite layer by a factor of 2.46, substantially mitigating the risk of thermal degradation.

4.2. Wind flow stress on the PSP at different inclination angles

The simulation findings regarding the wind flow across solar panels at various angles of inclination are depicted in figures 9 and 10. The simulations yield contour plots of pressure distribution on the solar panel, presented in figure 9, which illustrate changes in pressure with varying panel inclinations. Figures 10(a)–(c) further displays the pressure distribution on a hypothetical vertical plane perpendicular to the solar panel. The results indicate that the highest pressure on the solar panel occurs near the leading edge at the bottom surface, decreasing towards the trailing edge. When comparing the effects on solar panels inclined at 30°, 45°, and 60°, it is observed that the panel at 60° encounters the most intense wind pressure, with a peak pressure of 32.4 Pa localized at the panel's lower region. In contrast, a 30° inclination results in a more evenly distributed wind pressure with a peak

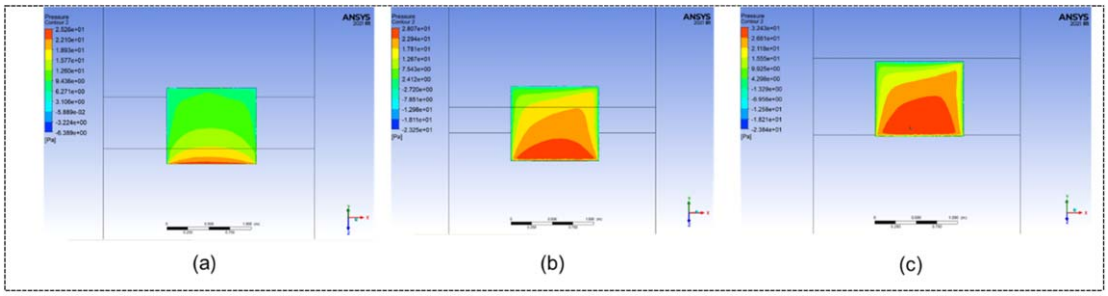

Figure 9. Contour plot pressure distribution on the solar panel with inclination angle of (a) 30°, (b) 45° and (c) 60°.

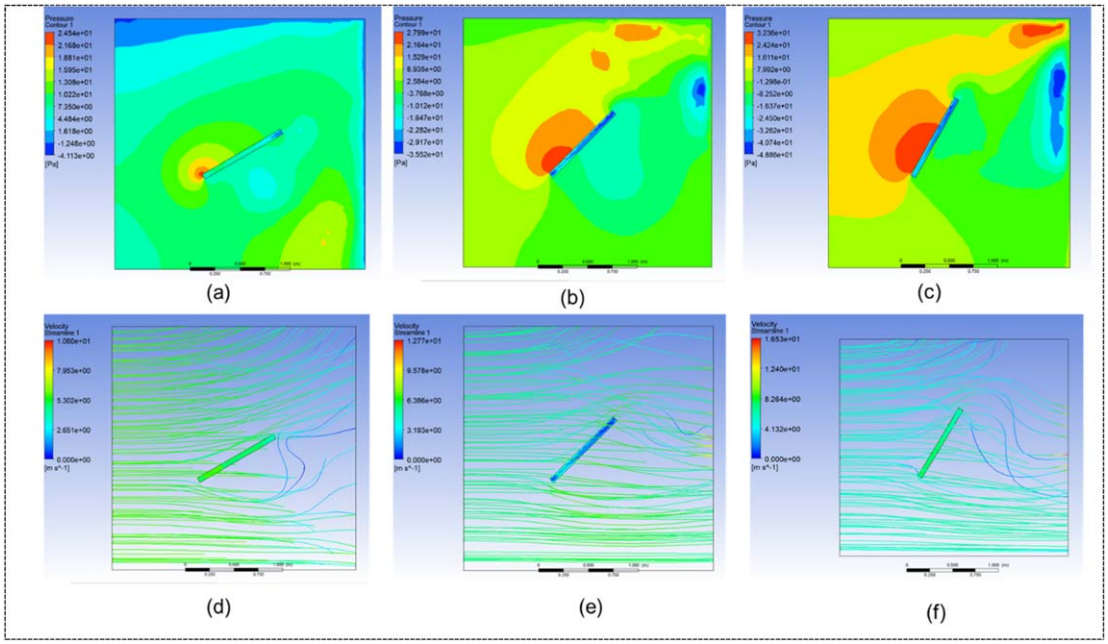

Figure 10. Y-Z vertical plane pressure distribution on the solar panel with inclination angle of (a) 30°, (b) 45° and (c) 60°, and a and streamline of flow with the inclination angle of (d) 30°, (e) 45° and (f) 60°.

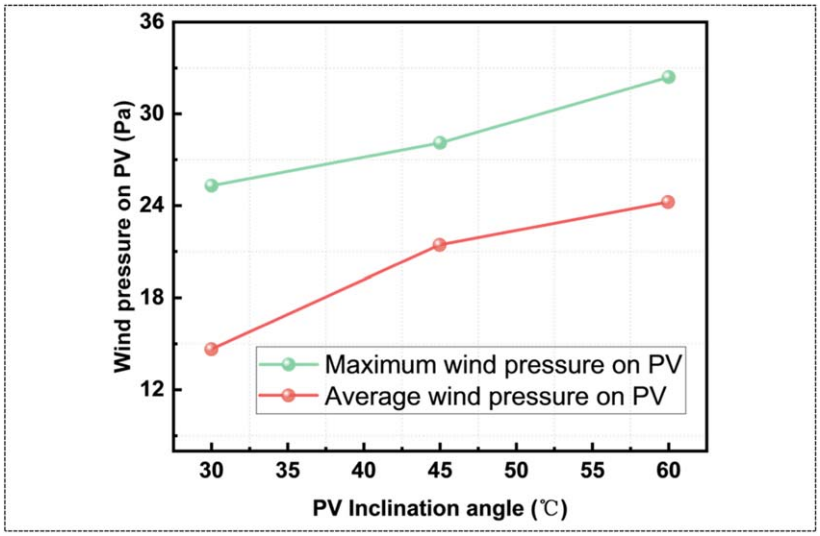

Figure 11. Plot of wind pressure on PV in terms of vertical inclination angle.

of 25.3 Pa. Streamline flow analyses from figures 10(d)–(f) corroborate that solar panels with lesser inclinations tend to exhibit improved mechanical stability against wind forces. Furthermore, figure 11 illustrates the general trend of wind pressure variation as a function of the panel's inclination angle. It is evident from the plot that the vertical pressure exerted on the PV panel is directly proportional to its angle of inclination. Consequently, to minimize wind pressure damage, solar panels should be positioned at a smaller inclination angle, considering the daily solar radiation azimuth.

Despite the successful establishment of the simulation and the attainment of anticipated results, this study presents several aspects that require optimization. Primarily, the study proposes to analyze the behavior of solar panels under varying wind velocities and temperature changes due to a specified radiation level. Nonetheless, the temperature analysis was conducted using a 'steady-state thermal' approach rather than integrating 'wind flow,' resulting in the simulation being divided into two discrete sub-sections. This division overlooks the interplay between wind flow and thermal variation. Additionally, the performance of the solar panels is subject to change with different wind velocities, a factor that has not been addressed within the scope of this paper.

5. Conclusion

In conclusion, this study has provided a comprehensive analysis of the thermal performance and mechanical resilience of perovskite solar modules under varying environmental conditions. FEM simulations were utilized to assess the impact of cooling systems on temperature regulation and the influence of wind velocity on structural integrity. The findings indicate that cooling systems are highly effective, reducing the perovskite layer's temperature significantly, by approximately 2.46 times, thus enhancing the operational stability of the panels. Moreover, it was determined that the wind pressure experienced by the panels increases with the angle of inclination, suggesting that lower angles are preferable for minimizing wind-related damage while optimizing energy capture based on solar azimuth patterns. However, the inherent instabilities of perovskite solar PV modules, coupled with the limitations in current material science advancements, present a notable challenge. The relatively lower thermal conductivity of perovskite, compared to traditional semiconductor materials, poses a substantial barrier to the commercialization of PSPs. This necessitates a collaborative effort among material researchers and engineers to develop viable solutions that bridge this significant gap.

Data availability statement

All data that support the findings of this study are included within the article (and any supplementary files).

Author contributions statement

Xinzhi Liu and **Ranfu Wang** have made equal contributions to this manuscript. Both were integrally involved in all stages of the study. Their efforts included initial conceptualization, design of the research, execution of simulations, data collection and analysis, as well as drafting and revising the manuscript. Their contributions are reflected equally across all aspects of this research. **Suhaidi Shafie** contributed significantly to the conceptualization and technical perspective of the research. He also played a key role in structuring the manuscript, drafting initial versions, and critically revising the content to enhance its scholarly value.

ORCID iDs

Xinzhi Liu https://orcid.org/0000-0002-8032-0965
Suhaidi Shafie https://orcid.org/0000-0002-8867-2754

References

[1] Brockway P E, Owen A, Brand-Correa L I and Hardt L 2019 Estimation of global final-stage energy-return-on-investment for fossil fuels with comparison to renewable energy sources *Nat. Energy* **4** 612–21
[2] Tiedje T, Yablonovitch E, Cody G D and Brooks B G 1984 Limiting efficiency of silicon solar cells *IEEE Trans. Electron Devices* **31** 711–6
[3] Manser J S, Christians J A and Kamat P V 2016 Intriguing optoelectronic properties of metal halide perovskites *Chem. Rev.* **116** 12956–3008
[4] Shi B, Duan L, Zhao Y, Luo J and Zhang X 2020 Semitransparent perovskite solar cells: from materials and devices to applications *Adv. Mater.* **32** 2
[5] Chen H *et al* 2020 Efficient bifacial passivation with crosslinked thioctic acid for high-performance methylammonium lead iodide perovskite solar cells *Adv. Mater.* **32** 2

[6] Chu Z, Yang M, Schulz P, Wu D, Ma X, Seifert E, Sun L, Li X, Zhu K and Lai K 2017 Impact of grain boundaries on efficiency and stability of organic-inorganic trihalide perovskites *Nat. Commun.* **8** 2230
[7] Razza S, Castro-Hermosa S, Di Carlo A and Brown T M 2016 Research update: large-area deposition, coating, printing, and processing techniques for the upscaling of perovskite solar cell technology *APL Mater.* **4** 091508
[8] Li X, Zhang F, Wang J, Tong J, Xu T and Zhu K 2021 On-device lead-absorbing tapes for sustainable perovskite solar cells *Nat. Sustain.* **4** 1038–41
[9] Armstrong S and Hurley W G 2010 A thermal model for photovoltaic panels under varying atmospheric conditions *Appl. Therm. Eng.* **30** 1488–95
[10] Mashrafi M, Anik M H K, Israt M F, Habib A and Islam S 2023 Modeling the path to >30% power conversion efficiency in perovskite solar cells with plasmonic nanoparticles *RSC Adv.* **13** 19447–54
[11] Pan H *et al* 2020 Advances in design engineering and merits of electron transporting layers in perovskite solar cells *Mater Horiz* **7** 2276–91
[12] Tan S *et al* 2022 Stability-limiting heterointerfaces of perovskite photovoltaics *Nature* **605** 268–73
[13] Petrus M L *et al* 2017 Capturing the sun: a review of the challenges and perspectives of perovskite solar cells *Adv. Energy Mater.* **7** 1700264
[14] He M *et al* 2017 Meniscus-assisted solution printing of large-grained perovskite films for high-efficiency solar cells *Nat. Commun.* **8** 16045
[15] Yang S *et al* 2019 Stabilizing halide perovskite surfaces for solar cell operation with wide-bandgap lead oxysalts *Science (1979)* **365** 473–8
[16] Hasan O, Arif A F M and Siddiqui M U 2012 Finite element modeling and analysis of photovoltaic modules *American Society of Mechanical Engineers* **8** 495–505
[17] Teo H G, Lee P S and Hawlader M N A 2012 An active cooling system for photovoltaic modules *Appl. Energy* **90** 309–15
[18] Zhe L W, Yusoff M I B, Misrun M I, Abdul Razak A B, Ibrahim S and Zhubir N S B 2016 Investigation of solar panel performance based on different wind velocity using ANSYS software *Indonesian Journal of Electrical Engineering and Computer Science* **1** 456
[19] Kumar Laha S, Kumar Sadhu P, Ganguly A and Kumar Naskar A 2022 A comparative study on thermal performance of a 3D model based solar photovoltaic panel through finite element analysis *Ain Shams Engineering Journal* **13** 101533
[20] Nivelle P, Tsanakas J A, Poortmans J and Daenen M 2021 Stress and strain within photovoltaic modules using the finite element method: a critical review *Renew. Sustain. Energy Rev.* **145** 111022
[21] Qian X, Gu X and Yang R 2016 Lattice thermal conductivity of organic-inorganic hybrid perovskite CH3NH3PbI3 *Appl. Phys. Lett.* **108**
[22] Duffie (Deceased) J A, Beckman W A and Blair N 2020 *Solar Engineering of Thermal Processes, Photovoltaics and Wind* (Wiley) (https://doi.org/10.1002/9781119540328)
[23] Chong K K and Wong C W 2009 General formula for on-axis sun-tracking system and its application in improving tracking accuracy of solar collector *Sol. Energy* **83** 298–305
[24] Fatemi S A and Kuh A 2013 Solar radiation forecasting using zenith angle *2013 IEEE Global Conf. on Signal and Information Processing* (IEEE) 523–6
[25] Heiderhoff R, Haeger T, Pourdavoud N, Hu T, Al-Khafaji M, Mayer A, Chen Y, Scheer H and Riedl T 2017 Thermal conductivity of methylammonium lead halide perovskite single crystals and thin films: a comparative study *The Journal of Physical Chemistry* C **121** 28306–11
[26] Choi S M, Park C-D, Cho S-H and Lim B-J 2022 Effects of wind loads on the solar panel array of a floating photovoltaic system—Experimental study and economic analysis, *Energy* **256** 124649